Role of compression metallization in UO2 fission-product energy cascade track: multiscale electron-phonon analyses

Woong-Kee Kim[a,c†], Corey Melnick[b,†], Ji Hoon Shim[c,d], Heajin Kim[d], Massoud Kaviany[b,c]

[a]*Department of Nuclear Engineering, Seoul National University, 1, Gwanak-ro, Gwanak-gu, Seoul, 08826, Korea*
[b]*Department of Mechanical Engineering, University of Michigan, Ann Arbor, Michigan 48109-2125, USA*
[c]*Division of Advanced Nuclear Engineering, Pohang University of Science and Technology, 77, Cheongam-ro, Nam-gu, Pohang-si, Gyeongsangbuk-do 37673, Korea*
[d]*Department of Chemistry, Pohang University of Science and Technology, 77, Cheongam-ro, Nam-gu, Pohang-si, Gyeongsangbuk-do 37673, Korea*

† *equally contributed to the work*

INTRODUCTION

We investigate the cascade of energy from the electron to atomic subsystems in UO_2, following the electronic stoppage of a swift heavy ion. In particular, we use a multiscale analysis to investigate the radiation damage which results from this energy cascade. We use *ab initio* (DFT-HSE) simulations to calculate the pressure and temperature dependent material properties of UO_2 in order to explore its transition from a dielectric to metal and the effects this has on nonequilibrium energy transport. Then, we use a combined mesoscale-atomistic model (TTM+MD) with a parameterization informed by the *ab initio* simulations in order to explore the mechanisms of radiation damage and validate our *ab initio* approximations.

UO_2 AB INITIO CALCULATIONS

In our *ab initio* simulations using the DFT-HSE framework, we support the previous suggestion [1] that UO_2 becomes metallic under high pressures (Fig.1).

Briefly, let us overview the remaining simulation methodology. For the electronic properties, we use the *ab initio* simulation code Quantum-Espresso [2,3] with a plane-wave basis set with a kinetic energy cut-off of 120 Ry. Scalar relativistic, norm-conserving Martins-Toullier [4] pseudopotentials are constructed for uranium, configuration $[Rn]5f^3 6d^1 7s^2$, and oxygen, configuration $[He]2s^2 2p^4$. The simulations are carried out on a 6×6×6 (6^3) κ_e-mesh with the HF exchange considered on a fully commensurate (6^3) q_e-mesh at each κ_e-point. When evaluating material properties like the density of states, heat capacity, thermal conductivity, or electron-phonon coupling, the resulting mesh of electron eigenvalues is interpolated onto a 30^3 κ_e-mesh. The ground state lattice constant, a = 5.66 Å, is found by comparing the crystal energy for variations. We do not include the spin-orbit coupling, as it would reduce our ability to simulate reasonably dense κ_e and q_e-meshes, particularly in our electron-phonon coupling simulations. Still, the electronic properties predicted within our simulations match reasonably well with those recorded in experiments and other, previously published *ab initio* calculations.

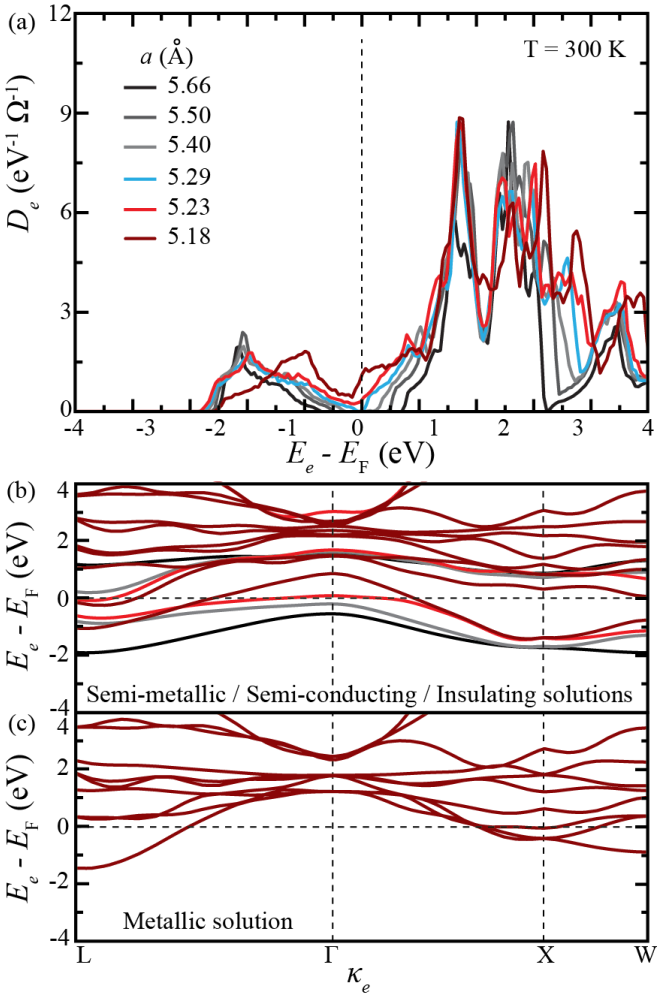

Figure 1. (a) Electron density of states and (b),(c) bandstructure of UO_2 for variations in the lattice constant, where only the first valence and conduction bands are shown for the semi-conducting and insulating UO_2.

Furthermore, we calculate the electronic heat capacity (Fig. 2) and thermal conductivity (Fig. 3), and the electron-phonon energy coupling (Fig. 4) of UO_2 for variations in the pressure and electron and phonon temperatures.

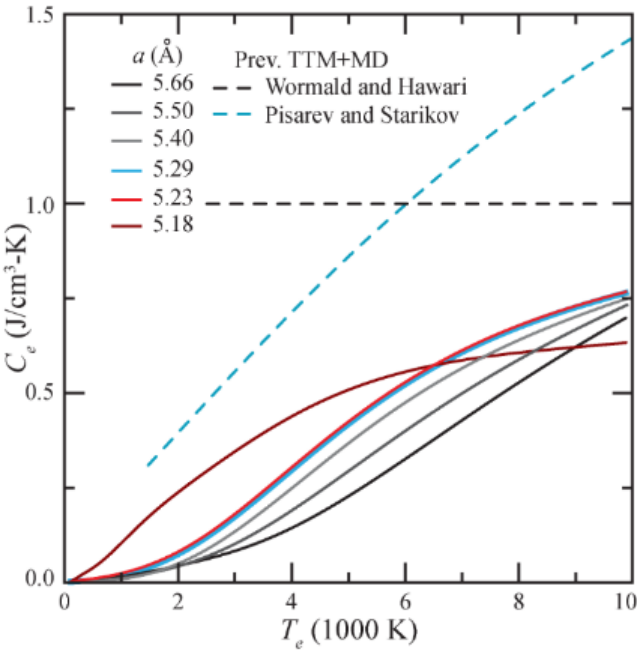

Figure 2. Heat capacity for variations in the electronic temperature and lattice parameter.

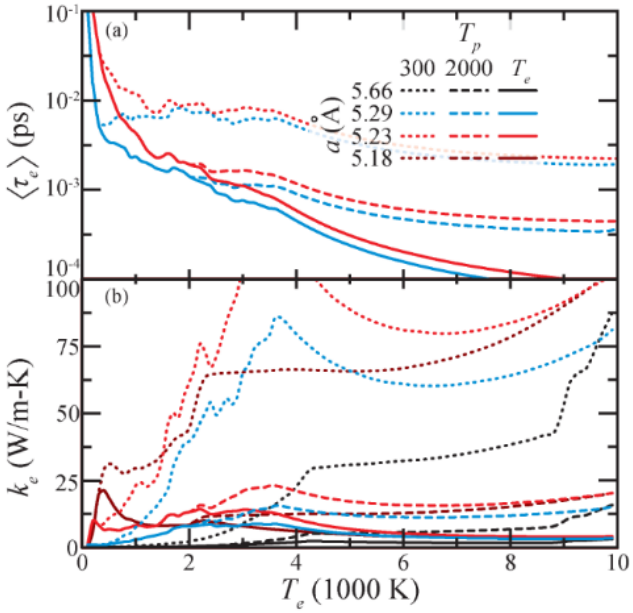

Figure 3. Electron lifetime (a) and thermal conductivity (b) for variations in the electron temperature and electron-phonon non-equilibrium. Under equilibrium conditions, the conductivity is suppressed by the very short electron lifetime.

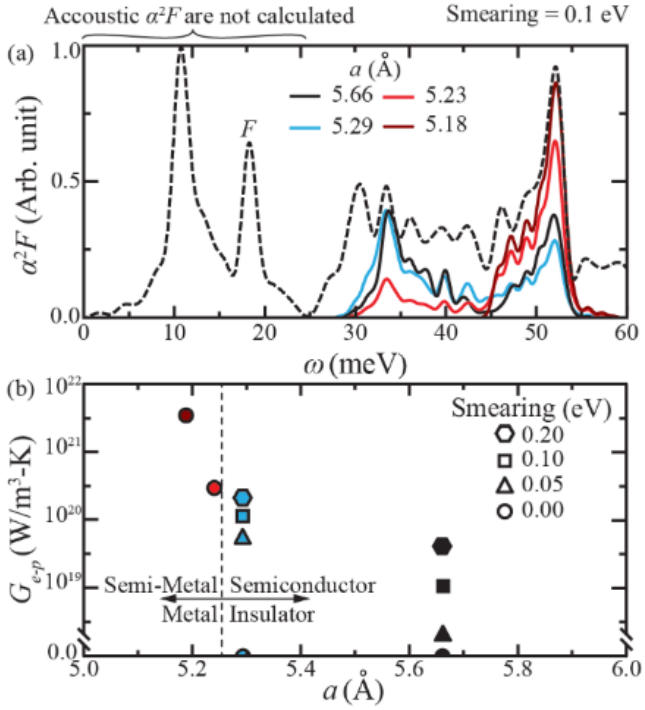

Figure 4. (a) Phonon spectral function and density of states, *F*. The spectral functions are normalized by their total integral, while the phonon density of states is scaled such that the spectral function curves reside within it. (b) The electron-phonon coupling for the optical phonon modes in UO_2.

We predict that pressurized, semi-metallic UO_2 is a relatively sluggish conductor due to its strong electron-phonon coupling. However, the large non-equilibrium between the electronic and phononic subsystems induced in UO_2 by the electronic stopping of a swift heavy ion enables fast thermal transport. Under such conditions, our *ab initio* simulations give us a range of parameterizations for our subsequent TTM+MD runs which enables their successful prediction of the track radius and threshold stopping power.

TTM+MD CALCULATIONS

the TTM+MD model, energy exchange between the two subsystems (electronic, *e*, and phononic, *p*) is specified by the electron heat diffusion equation [5],

$$C_e(T_e)\frac{\partial T_e}{\partial t} = \nabla(k_e \nabla T_e) - G_{e-p}(T_e - T_p) + G_e T_p', \quad (12)$$

where C_e, k_e and T are the heat capacity, number density, thermal conductivity and temperature, respectively. T_p' is the local temperature of atoms whose velocity is greater the electronic stopping critical velocity. $G_{e\text{-}p}$ is the electron-phonon coupling constant, and G_e is the electron stopping constant obtained from electronic stoppage calculation by SRIM [6]. Given an updated distribution of the phonon temperature (T_p), the spatial and temporal distributions of non-equilibrium electron temperature (T_e) are solved numerically using a finite difference method. Where the

typical TTM model uses a heat diffusion equation for the phonon temperature, the TTM+MD model replaces this with the Langevin dynamics, as we discuss next.

Within the Langevin dynamics, the movement of atom *i* is governed by [5,7]

$$\boldsymbol{F}_i = -\frac{\partial U}{\partial \boldsymbol{r}_i} - \gamma \boldsymbol{v}_i + \boldsymbol{F}'_{lang}(t), \qquad (13)$$

where $\boldsymbol{F}_i$ is total force acting on atom *i*, *U* is the interatomic potential, γ is the friction-coefficient, and $\boldsymbol{F}'_{lang}$ is the stochastic Langevin force term.

We perform the TTM+MD simulations in a box with dimensions of 32.8×32.8×10.9 nm^3, corresponding to a 60×60 ×20 supercell with 864,000 ions [Fig. 12(a)], and we discretize this simulation box into a 31×31×7 mesh for the finite difference integration of the electron energy equation. We use the CRG interatomic potential[8] based on embedded-atom method (EAM) for short-range forces, which have been actively applied to thermal transport and defect dynamics, and the long-range charge summation method PPPM for the long-range forces.The LAMMPS simulation package is used to integrate the Langevin dynamics and the coupled electron energy equation [Eq. (12)]. To initialize our system, we equilibrate a NPT ensemble of UO_2 atoms at 300 K for 1 ns with a 1 fs time step. Next, the initial electronic temperature is prescribed in order to mimic the electronic system in the wake of a swift heavy ion. Here we assume that initial heat spike morphology is cylindrically symmetric in the *z*-direction and is given by a Gaussian distribution. This Gaussian distribution is determined using a modified form of the analytical thermal spike model (ATSM) [9–12]. That is,

$$\Delta T_e = \frac{S_e}{\rho_e c_e \pi \mu_e^2} \exp\left(-\frac{r^2}{\mu_e^2}\right), \qquad (21)$$

where S_e is the initial energy deposited as a heat spike in the electronic subsystem, ρ_e and c_e are the electronic density and electronic specific heat, and μ_e is depends on the thermal diffusivity of electrons, and we assume that it is 2 nm

After the irradiation simulation by initial electronic temperature, the amorphized and defective ion track remains distinct, as shown in Fig. 5.

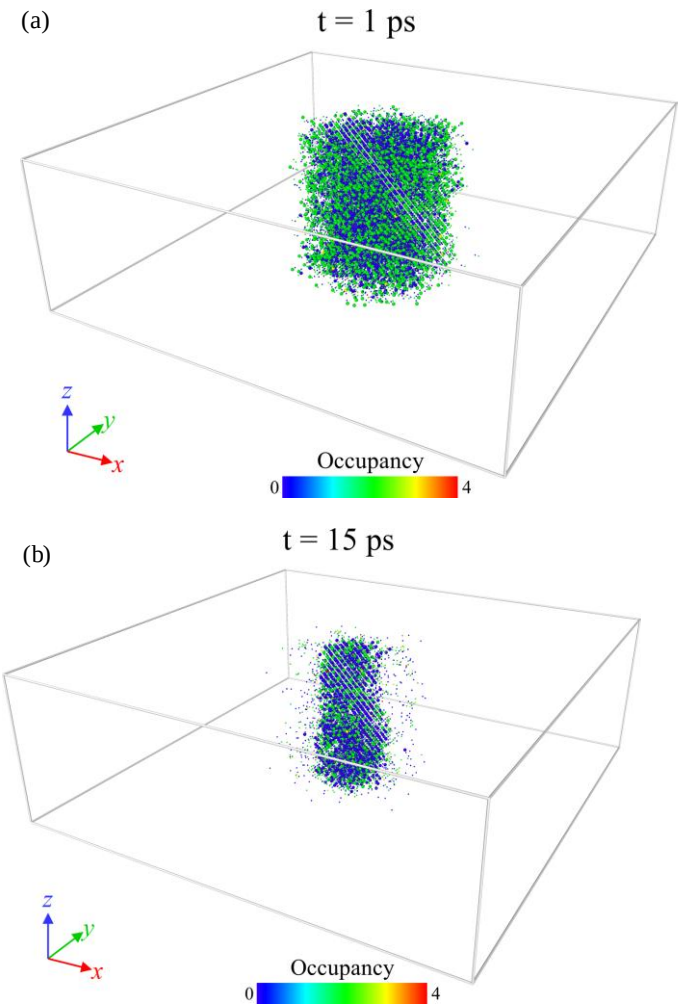

Figure 5. Defect distribution within the simulation box after elapsed times of (a) 1 ps and (b) 15 ps following a 29 keV/nm energy deposition.

RESULTS

These TTM+MD runs, in addition to accurately reproducing the experimental observations (Fig. 6), provide a wealth of information on the damage processes which follow electronic stopping.

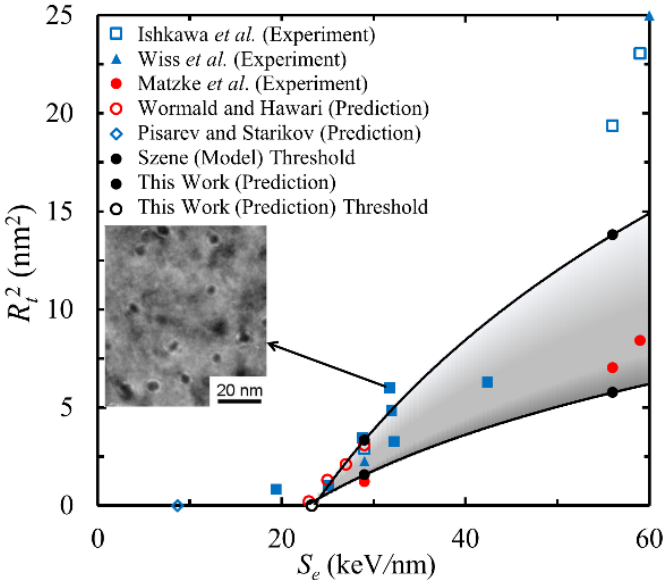

Figure 6. Square of the track radius as a function of stopping loss (S_e) in irradiated UO_2. Blue squares and red circles denote experimental results and predictions. (The inset TEM image is from Ishkawa *et al.* [13]).

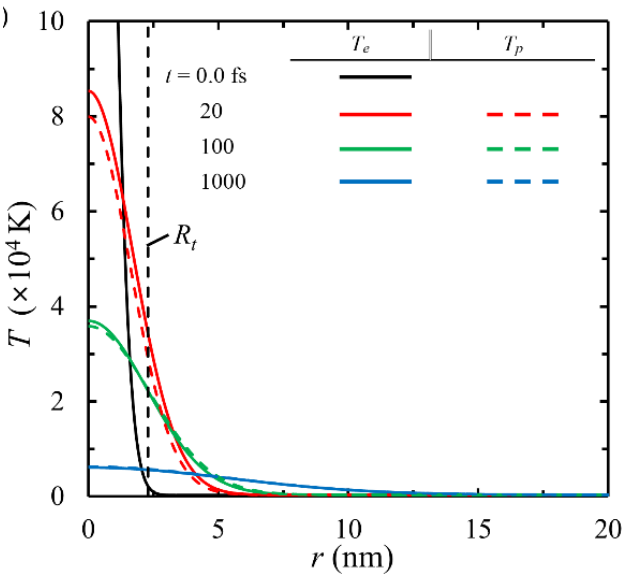

Figure 7. Spatial and temporal variation of temperature, pressure and defects following a 29 keV/nm energy deposition and (a) Pressure at a few selected times for variations in the distance from the ion track (averaged). (b) Temperatures of the electron and phonon subsystems at few selected times for variations in the distance from the ion track

In particular, we report the fs-scale evolution of the pressure [(Fig. 7(a)] and the subsystem temperatures [(Fig. 7(b)] in the wake of a swift heavy ion penetrating UO_2.

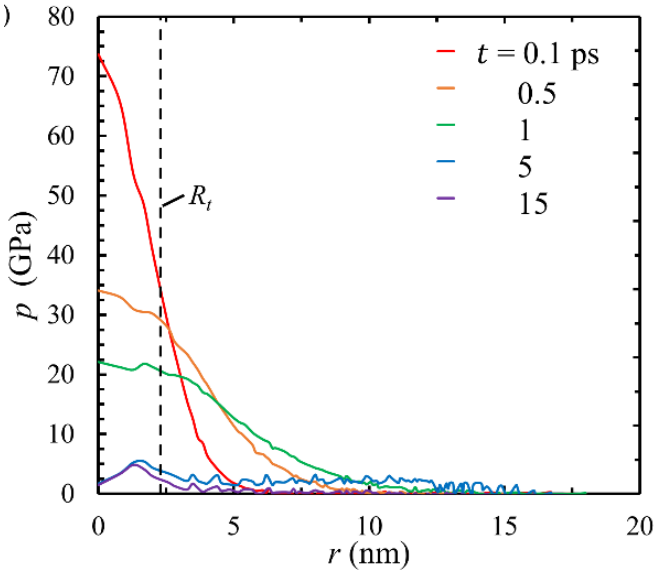

These analyses support the potential formation of a metallic UO_2 phase with good thermal transport. However, the track is amorphous and U-heavy, rather than crystalline, compressed UO_2. Additionally, the TTM+MD simulations use a set of constant-value, rather than pressure and temperature dependent, material properties. Thus, the multiscale analysis only gives a plausible explanation of the apparent, metallic behavior, and it only provides a rough outline of the energy cascade and damage which follows swift heavy ion penetration. With these caveats, our analysis still provides useful results.

Let us expand our defect characterization and quantify the penetration depth of an incident ion using TTM+MD. To do this, we discretize the stopping energy loss relation calculated within SRIM [Fig. 15(a)] for a typical fission fragment produced by the fission of U^{235} following its capture of a thermal neutron. That is, we simulate the stoppage of Xe^{133} with 76 MeV of initial kinetic energy [14], rather than use the ions used in previous experiments (Xe^{129} or U^{238}). Then, we use TTM+MD to calculate the number of defects produced along the particle track. Next, we convert from the energy loss domain to a physical, penetration depth domain. Finally, we compare the SRIM and TTM+MD predictions of defect production per distance. Again, and as shown in Fig. 15(b), the TTM+MD model predicts that many more defects are created during electronic stopping than the SRIM simulations predict. Near the threshold stopping power, however, both models predict a similar number of defects are created along the ion track. Thus, we hypothesize that the SRIM model underestimates the number of defects created during the

electronic stoppage, while overestimating the number of defects created during nuclear stoppage (due to non-existence of molecular dynamics in SRIM). Indeed, while the TTM+MD framework is explicitly built to capture the electron-phonon coupling, the large flow of energy from the electronic to phononic subsystems thereby, the massive pressure and temperature induced in the lattice, and the defects which result from these phenomena; SRIM is not.

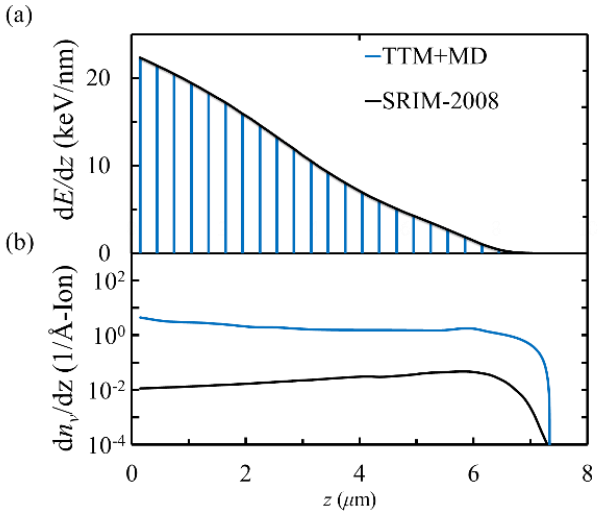

Figure 15. (a) Electronic stopping loss of Xe^{133} ion having 76 MeV of initial energy along the penetration path in UO_2 (Black line) calculated by SRIM codes and the discretization of the stopping power for input of TTM+MD simulations (Blue bars). (b) Comparison of resultant defect formation per depth of penetration by SRIM (Black line) and TTM+MD (Blue line).

Note that the spatial distribution of atomic displacements per atom (dpa) along the path of the incident particle is an important description of the effective radiation damage at the engineering scale. It is given by

$$\mathrm{dpa}(z) = \frac{\Phi(z)}{n_p}\frac{\mathrm{d}n_v(z)}{\mathrm{d}z}, \qquad (22)$$

where Φ, n_p, $\mathrm{d}n_v/\mathrm{d}z$ are the predetermined ion fluence distribution, atom number density and defect formation per distance, respectively. As we hypothesize that SRIM substantially underestimates the latter quantity, and that TTM+MD represents a substantial improvement over the SRIM model, we suggest that nuclear engineers adopt of TTM+MD as the standard when evaluating the dpa of nuclear-related materials.

CONCLUSIONS

We investigate the cascade of energy from the electron to atomic subsystems in UO_2, following the electronic stoppage of a swift heavy ion. In particular, we use a multiscale analysis to investigate the radiation damage which results from this energy cascade. We use *ab initio* (DFT-HSE) simulations to calculate the pressure and temperature dependent material properties of UO_2 in order to explore its transition from a dielectric to metal and the effects this has on nonequilibrium energy transport. Then, we use a combined macroscale-atomistic model (TTM+MD) with a parameterization informed by the aforementioned *ab initio* simulations in order to explore the mechanisms of radiation damage and validate our *ab initio* approximations.

In our *ab initio* simulations using the DFT-HSE framework, we support the previous suggestion that UO_2 becomes metallic under high pressures. Furthermore, we calculate the electronic heat capacity and thermal conductivity, and the electron-phonon energy coupling of UO_2 for variations in the pressure and electron and phonon temperatures. We predict that pressurized, semi-metallic UO_2 is a relatively sluggish conductor due to its strong electron-phonon coupling. However, the large non-equilibrium between the electronic and phononic subsystems induced in UO_2 by the electronic stopping of a swift heavy ion enables fast thermal transport. Under such conditions, our *ab initio* simulations give us a range of parameterizations for our subsequent TTM+MD runs which enables their successful prediction of the track radius and threshold stopping power. From these predicted results that ground state, with k_e = 5.6 W/m-K, and $G_{e\text{-}p} = 10^{17}$ W/m^3-K, and the transition state with k_e = 47 W/m-K, and $G_{e\text{-}p} = 10^{18}$ W/m^3-K, both result in track radii in good agreement with the experimental results. These TTM+MD runs, in addition to accurately reproducing the aforementioned experimental observations, provide a wealth of information on the damage processes which follow electronic stopping. In particular, we report the fs-scale evolution of the pressure, the subsystem temperatures, and the production and recombination of defects in the wake of a swift heavy ion penetrating UO_2. These analyses support the potential formation of a metallic UO_2 phase with good thermal transport. However, the track is amorphous and U-heavy, rather than crystalline, compressed UO_2. Additionally, the TTM+MD simulations use a set of constant-value, rather than pressure and temperature dependent, material properties. Thus, the multiscale analysis only gives a plausible explanation of the apparent, metallic behavior, and it only provides a rough outline of the energy cascade and damage which follows swift heavy ion penetration. With these caveats, our analysis still provides useful results.

In particular, we evaluate the defect creation from electronic stoppage along the particle path by

transforming the TTM+MD simulations from the damage-per-energy to a damage-per-length scale and show its applicability to the dpa evaluation over the μm-scale of the ion track using our nm-scale TTM+MD simulations. This analysis shows that much more damage occurs within the radiation track during electronic stopping than is predicted within the more common SRIM model. We show that this increase in damage is due to the electron-phonon coupling, which is not captured within the SRIM model. Indeed, if combined with the existing collision cascade MD simulation for nuclear stoppage, we propose that the TTM+MD framework can be used for a more accurate approach to evaluating the overall dpa of the irradiated material by both the electronic and nuclear stoppage. This framework, based on multiscale approach, is applicable to other metallic alloys under fission, fusion or irradiation by incident ions.

REFERENCES

[1] L. Huang, Y. Wang, P. Werner, Orbital-Selective Mott Transition and Evolution of the Zhang-Rice State in Cubic Phase UO 2 Under Pressure, arXiv Prepr. arXiv1506.06548. (2015) 3–7.

[2] P. Giannozzi, O. Andreussi, T. Brumme, O. Bunau, M.B. Nardelli, M. Calandra, R. Car, C. Cavazzoni, D. Ceresoli, M. Cococcioni, Advanced capabilities for materials modelling with Quantum ESPRESSO, J. Phys. Condens. Matter. 29 (2017) 465901.

[3] P. Giannozzi, S. Baroni, N. Bonini, M. Calandra, R. Car, C. Cavazzoni, D. Ceresoli, G.L. Chiarotti, M. Cococcioni, I. Dabo, A.D. Corso, S. de Gironcoli, S. Fabris, G. Fratesi, R. Gebauer, U. Gerstmann, C. Gougoussis, A. Kokalj, M. Lazzeri, L. Martin-Samos, N. Marzari, F. Mauri, R. Mazzarello, S. Paolini, A. Pasquarello, L. Paulatto, C. Sbraccia, S. Scandolo, G. Sclauzero, A.P. Seitsonen, A. Smogunov, P. Umari, R.M. Wentzcovitch, QUANTUM ESPRESSO: a modular and open-source software project for quantum simulations of materials, J. Phys. Condens. Matter. 21 (2009) 395502. http://stacks.iop.org/0953-8984/21/i=39/a=395502.

[4] N. Troullier, J.L. Martins, Efficient pseudopotentials for plane-wave calculations, Phys. Rev. B. 43 (1991) 1993.

[5] D.M. Duffy, a M. Rutherford, Including the effects of electronic stopping and electron–ion interactions in radiation damage simulations, J. Phys. Condens. Matter. 19 (2007) 16207. doi:10.1088/0953-8984/19/1/016207.

[6] J.F. Ziegler, M.D. Ziegler, J.P. Biersack, SRIM: the stopping and range of ions in matter, Nucl. Instruments Methods Phys. Res. Sect. B Beam Interact. with Mater. Atoms. 268 (2010) 1818–1823. doi:10.1016/j.nimb.2010.02.091.

[7] A. Rutherford, D. Duffy, The effect of electron-ion interactions on radiation damage simulations, J. Phys. Condens. Matter. 19 (2007) 1–9. doi:10.1088/0953-8984/19/49/496201.

[8] M.W.D. Cooper, M.J.D. Rushton, R.W. Grimes, A many-body potential approach to modelling the thermomechanical properties of actinide oxides, J. Phys. Condens. Matter. 26 (2014) 105401. doi:10.1088/0953-8984/26/10/105401.

[9] G. Szenes, General features of latent track formation in magnetic insulators irradiated with swift heavy ions, Phys. Rev. B. 51 (1995) 8026–8029. doi:10.1103/PhysRevB.51.8026.

[10] G. Szenes, Thermal spike model of amorphous track formation in insulators irradiated by swift heavy ions, Nucl. Instruments Methods Phys. Res. Sect. B Beam Interact. with Mater. Atoms. 116 (1996) 141–144. doi:10.1016/0168-583X(96)00025-0.

[11] G. Szenes, Comparison of two thermal spike models for ion-solid interaction, Nucl. Instruments Methods Phys. Res. Sect. B Beam Interact. with Mater. Atoms. 269 (2011) 174–179. doi:10.1016/j.nimb.2010.11.009.

[12] G. Szenes, Ion-induced amorphization in ceramic materials, J. Nucl. Mater. 336 (2005) 81–89. doi:10.1016/j.jnucmat.2004.09.004.

[13] N. Ishikawa, T. Sonoda, T. Sawabe, H. Sugai, M. Sataka, Electronic stopping power dependence of ion-track size in UO2 irradiated with heavy ions in the energy range of ~1 MeV/u, Nucl. Instruments Methods Phys. Res. Sect. B Beam Interact. with Mater. Atoms. 314 (2013) 180–184. doi:10.1016/j.nimb.2013.05.038.

[14] J. Randrup, R. Vogt, Calculation of fission observables through event-by-event simulation, Phys. Rev. C - Nucl. Phys. 80 (2009) 1–11. doi:10.1103/PhysRevC.80.024601.